Sea ice and iceberg dynamic interaction

Elizabeth C. Hunke[1] and Darin Comeau[2]

Received 10 August 2010; revised 3 January 2011; accepted 23 February 2011; published 14 May 2011.

[1] A model of iceberg motion has been implemented in the Los Alamos sea ice model (CICE). Individual bergs are tracked under the influence of winds, currents, sea surface tilt, Coriolis, and sea ice forcing. In turn, sea ice is affected by the presence of icebergs, primarily as obstacles that cause the sea ice to ridge on the upstream side or create open water on the downstream side of the bergs. Open water formed near icebergs due to sea ice ridging and blocking of sea ice advection increases level and ridged ice downstream of the bergs through increased frazil ice formation. Resulting anomalies in sea ice area and thickness (compared with a simulation without icebergs) are transported with the sea ice flow, expanding over time. Although local changes in the sea ice distribution may be important for smaller-scale studies, these anomalies are small compared with the total volume of sea ice and their effect on climate-scale variables appears to be insignificant.

Citation: Hunke, E. C., and D. Comeau (2011), Sea ice and iceberg dynamic interaction, *J. Geophys. Res.*, *116*, C05008, doi:10.1029/2010JC006588.

1. Introduction

[2] Icebergs populate high-latitude seas in both hemispheres and have drawn scientific interest for several reasons. Icebergs in the western North Atlantic Ocean, which pose a threat to shipping and resource extraction, receive a great deal of attention from monitoring agencies such as the International Ice Patrol and from modelers striving to predict their tracks. As conduits for freshwater transport, icebergs modify oceanic water mass properties and therefore have ramifications for biological communities and the physical climate system. While large numbers of small bergs thus influence both hemispheres, the southern hemisphere also features "giant" icebergs more than 10 nautical miles (1 nautical mile = 1.852 km) in horizontal extent that are responsible for approximately half of the fresh watershed from the Antarctic continent [*Silva et al.*, 2006].

[3] Depending on the motivating goal, two approaches have generally been taken in iceberg dynamic modeling efforts: treat the icebergs as a statistical distribution or model and track each berg individually. For studies of meltwater distribution that must necessarily include many small bergs, the former approach is natural [e.g., *Bigg et al.*, 1997; *Gladstone et al.*, 2001; *Jacka and Giles*, 2007; *Jongma et al.*, 2009]. The latter approach is used for prediction of berg trajectories in regions of high maritime traffic [e.g., *Smith and Banke*, 1983; *Smith*, 1993; *Kubat et al.*, 2005] and for some giant icebergs in the Southern Ocean [e.g., *Lichey and Hellmer*, 2001].

[1]Fluid Dynamics and Solid Mechanics Group, Theoretical Division, Los Alamos National Laboratory, Los Alamos, New Mexico, USA.

[2]Program in Applied Mathematics, University of Arizona, Tucson, Arizona, USA.

0148-0227/11/2010JC006588

[4] Although many of these studies include sea ice as one of the forcing influences on iceberg momentum, only *Jongma et al.* [2009] mention the potential effect that icebergs may have on sea ice. In their study, icebergs distribute meltwater nonuniformly over the ocean surface, which subsequently affects the area and thickness distribution of sea ice; stabilization of the water column by fresh, cold iceberg meltwater leads to greater sea ice area, which then contributes to further cooling and freshening of the surface ocean. They do not include any direct effects on sea ice through dynamical interaction with the bergs. In another modeling study using an early version of CICE, *Hunke and Ackley* [2001] found that sea ice advection created polynas in the lee of icebergs, as they had observed previously in the Weddell Sea. Icebergs in that study were treated as islands in the model's land mask, however.

[5] Thus icebergs can affect sea ice behavior, not just through indirect effects such as ocean surface temperature or salinity, but also through direct contact. A deleterious example occurred during the first 5 years of this century, when several large icebergs calved and were trapped in the southern Ross Sea. The icebergs prevented the normal spring breakout of sea ice behind them [*Brunt et al.*, 2006] and strongly impacted nearby penguin colonies [*Ainley et al.*, 2006].

[6] The present study explores the dynamical interaction of icebergs and sea ice and the effect of a few giant icebergs on properties of the sea ice pack in the Weddell Sea. We present, for the first time, a method for including icebergs in the simulation of sea ice dynamics, and we evaluate the effects thereof. The icebergs are not treated as sea ice; that is, they are not assigned to a sea ice thickness category and they do not have the same thermodynamic properties of sea ice. Instead, the icebergs are treated as coherent, individual ice volumes whose center of mass is tracked in a Lagrangian manner on the grid. Icebergs and sea ice have separate

Table 1. Constants Used in the Iceberg Calculations[a]

Symbol	Definition	Value
h_b	berg height	225 m
A_h	berg horizontal area	686 km^2
ρ_b	berg density	900 kg m^{-3}
ρ_s	snow density	300 kg m^{-3}
ρ_i	sea ice density	900 kg m^{-3}
ρ_w	ocean density	1025 kg m^{-3}
Ω	angular velocity	7.292×10^{-5} rad s^{-1}
c_i	sea ice coefficient of resistance	1
c_a	atmosphere coefficient of resistance	0.4
c_w	ocean coefficient of resistance	0.85
c_{da}	atmosphere drag coefficient	2.5×10^{-4}
c_{dw}	ocean drag coefficient	5×10^{-4}
P_s	critical sea ice strength	1×10^4 N m^{-1}
Δt_b	berg time step	2 min
Δt_i	sea ice time step	1 h

[a]All sea ice parameters are set as done by *Hunke and Lipscomb* [2008] and *Hunke* [2010].

momentum equations that are coupled through a bulk forcing term describing the horizontal momentum transfer between bergs and sea ice.

[7] First we describe the iceberg parameterization itself, then the changes made in the sea ice model. Simulation results for four giant icebergs placed in the Weddell Sea and tracked for 3 years are described in section 3, along with a number of sensitivity tests. These simulations indicate that the dynamic interaction of icebergs and sea ice is not important for the large-scale sea ice simulation, although local, physically intuitive changes do appear within the simulated sea ice pack. We discuss this finding and its consequences in section 4.

2. Model Description

[8] The iceberg parameterization is implemented in the Los Alamos sea ice model, CICE version 4.0, and run on a global, 1° mesh whose north pole is displaced into Greenland [*Hunke and Lipscomb*, 2008; *Hunke*, 2010]. A modified version of the Common Ocean Reference Experiments (CORE) [*Griffies et al.*, 2009] atmospheric forcing fields for 1990–1992 is applied, along with radiation fields as specified by the Arctic Ocean Model Intercomparison Project [*Hunke and Holland*, 2007]. The 6 hourly atmospheric forcing is interpolated to the sea ice time step (1 h). Ocean data, including full depth currents, are taken from the CCSM3 1990 control run (b30.009) [*Collins et al.*, 2006], averaged over 20 years into an annual climatology of monthly values. All forcing, parameters and other configuration choices in CICE are identical to the "ocnheat" case of *Hunke* [2010].

2.1. Icebergs

[9] Although our approach used for modeling icebergs is not new, we describe it here for completeness and to point out aspects that we have changed from previous studies. Following *Lichey and Hellmer* [2001], the momentum equation for iceberg motion is

$$M\frac{d\mathbf{u}_b}{dt} = \mathbf{F}_a + \mathbf{F}_w + \mathbf{F}_c + \mathbf{F}_{si} + \mathbf{F}_{ss}, \qquad (1)$$

where M is the iceberg mass, $\mathbf{u}_b$ is its velocity, t is time, and the terms on the right-hand side represent body or surface forcing by the atmosphere, ocean, Coriolis, sea ice, and sea surface slope, respectively. The Coriolis term takes the form

$$\mathbf{F}_c = -2M\Omega\sin\phi\hat{\mathbf{k}} \times \mathbf{u}_b = -Mf\hat{\mathbf{k}} \times \mathbf{u}_b$$

for latitude ϕ, where $\hat{\mathbf{k}}$ is the vertical unit vector. (Constant values are found in Table 1.) A geostrophic approximation gives the sea surface slope term a similar form

$$\mathbf{F}_{ss} = Mf\hat{\mathbf{k}} \times \mathbf{u}_w,$$

where $\mathbf{u}_w$ is the ocean current. $\mathbf{F}_c$ and $\mathbf{F}_{ss}$ dominate the momentum balance for the icebergs simulated here.

[10] Drag by wind and currents, $\mathbf{F}_a$ and $\mathbf{F}_w$, take the quadratic form

$$\mathbf{F}_a = \left(\frac{1}{2}\rho_a c_a A_{va} + \rho_a c_{da} A_{ha}\right)|\mathbf{u}_a - \mathbf{u}_b|(\mathbf{u}_a - \mathbf{u}_b) \qquad (2)$$

$$\mathbf{F}_w = \left(\frac{1}{2}\rho_w c_w A_{vw} + \rho_a c_{dw} A_{hw}\right)|\mathbf{u}_w - \mathbf{u}_b|(\mathbf{u}_w - \mathbf{u}_b), \qquad (3)$$

where A_{va} and A_{vw} represent the vertical surface area of the iceberg in contact with air and water, respectively. Likewise, A_{ha} and A_{hw} represent the horizontal surface area of the iceberg in contact with air and water. Full depth ocean currents are available; currents from the surface to the iceberg depth are vector averaged vertically for $\mathbf{u}_w$. The water drag term (3) could be computed at each level for which we have ocean current vectors, but *Kubat et al.* [2005] found that this did not significantly improve their simulation and we have chosen the simpler approach.

[11] The sea ice term follows that of *Lichey and Hellmer* [2001], whose expression depends on the sea ice area, a_i, strength P, and a critical strength parameter P_s,

$$\mathbf{F}_{si} = \begin{cases} 0, & a_i < 15\% \\ \frac{1}{2}\rho_i c_i A_{vsi}|\mathbf{u}_i - \mathbf{u}_b|(\mathbf{u}_i - \mathbf{u}_b), & 15\% < a_i \le 90\% \text{ or } P \le P_s. \end{cases} \qquad (4)$$

When the sea ice is highly concentrated and strong ($a_i >$ 90% and $P > P_s$), the iceberg momentum equation (1) is not used; instead the iceberg is "captured" by the sea ice: $\mathbf{u}_b = \mathbf{u}_i$, which *Lichey and Hellmer* [2001] found necessary for large, tabular bergs. While we do not attempt to tune air and drag coefficients to compensate for forcing and other model errors [*Smith and Banke*, 1983; *Smith*, 1993; *Keghouche et al.*, 2009], we do depart from the value of P_s used by *Lichey and Hellmer* [2001]. The sea ice strength parameterization used in CICE [*Lipscomb et al.*, 2007] yields slightly lower ice strengths than theirs [*Hibler*, 1979] for the same sea ice distribution, and therefore our critical strength value P_s is lower than theirs, 1.0×10^4 N m^{-1} as opposed to 1.3×10^4 N m^{-1}.

[12] Sea ice drag sometimes is not included in iceberg dynamics models at all, especially those in the North Atlantic [*Smith and Banke*, 1983; *Smith*, 1993]. In their northern hemisphere studies, which included the Arctic

Ocean, *Bigg et al.* [1996, 1997] included the drag but no capturing mechanism. Likewise, *Jongma et al.* [2009] also did not allow sea ice to capture icebergs in their model, which was based on that of *Bigg et al.* [1996]. However, *Schodlok et al.* [2006] show distinct, coherent patterns of sea ice and iceberg drift, indicating that such a capturing mechanism is appropriate for simulations of the Weddell Sea.

[13] Wave radiation forces can be significant for smaller bergs, but the ratio of wind drag to that force is proportional to the iceberg freeboard [*Savage*, 2001], and thus the wave radiation force is quite small for large (tall) icebergs. We neglect it here. We also ignore tidal effects [*MacAyeal et al.*, 2008; *Keghouche et al.*, 2009] and "added mass" associated with entrainment of water into the iceberg wake [e.g., *Savage*, 2001].

[14] The sea ice velocity and ocean currents are interpolated from the four corners of the grid cell in which the iceberg is located using inverse area weighting factors. The same factors are reused to extrapolate berg information to the grid cell corners, when needed. This is a basic particle-in-cell method [e.g., *Harlow*, 1955].

[15] Since we are focused on the dynamic interaction of icebergs and sea ice here, we ignore iceberg thermodynamic changes. (*Bigg et al.* [1996] note that melting affects iceberg trajectories, but in their tests, *Lichey and Hellmer* [2001] find that their iceberg tracks are not significantly altered when they change the draft by 100–400 m in their model, which does not incorporate thermodynamics.) For simplicity, we compute geometrical iceberg quantities assuming cylindrical bergs with a given horizontal area and height. Archimedes' Principle provides the vertical berg lengths in contact with water (h_{bw}), sea ice (h_{bi}), and air (h_{ba})

$$
\begin{aligned}
h_{bw} &= [(\rho_s h_{bs} + \rho_b h_b) - (\rho_s h_s + \rho_i h_i)]/\rho_w, \\
h_{bi} &= h_i, \\
h_{ba} &= h_b - (h_{bi} + h_{bw}).
\end{aligned}
$$

Here, ρ_b, ρ_w, ρ_i, and ρ_s are the densities of ice bergs, seawater, sea ice, and snow, respectively, and h_b, h_i, and h_s are the berg thickness, sea ice thickness, and snow depth on sea ice, respectively. Currently, the snow depth on icebergs, h_{bs}, is zero.

[16] While observations indicate that ice bergs tend to be elongated in shape rather than cylindrical, they also tend to align with the flow [e.g., *Bigg et al.*, 1997], and previous modeling studies have assumed a fixed angle between the long axis and the flow direction [*Bigg et al.*, 1997; *Lichey and Hellmer*, 2001]. Moreover, for motion of very large bergs the dominant force balance is between those terms that scale with mass (Coriolis and sea surface tilt terms). Therefore differences in surface area normal to the other forcing components (wind, sea ice and ocean stress) due to variations in berg shape are not likely to be significant in the present study.

[17] The iceberg momentum equation (1) is solved numerically using a simple predictor-corrector method consisting of a forward Euler prediction followed by backward Euler correction, with a time step of 2 minutes. Iceberg velocities are initialized to the sea ice velocity, interpolated to the berg location.

[18] Bergs may overlap grid cell edges, but they are prevented from entering grid cells that do not have enough open space to contain the portion of the berg that would otherwise enter, for instance when the grid cell is occupied with other bergs. Similarly, when an iceberg encounters land, either the coast or the seafloor, it stops. It may begin moving again with a change in directional forcing.

[19] A bathymetry data set used with the present grid and in the CCSM ocean data file defines the ocean depth at 40 levels, which vary in thickness from 10 m at the surface to 250 m in the deepest parts of the world ocean. Topography was created by merging the Arctic data from *Jakobsson et al.* [2000], *Smith and Sandwell* [1997] data from 72S to 72N, and Southern Ocean data from *Lythe and Vaughan* [2001], followed by pointwise modifications of important sills and channels that may have been smoothed by interpolation to the grid.

2.2. Sea Ice

[20] As our simulations will demonstrate, large icebergs often move more slowly than the sea ice surrounding them, due to their mass. The effect of an iceberg on the surrounding sea ice falls into one of two categories, depending on the relative motion between the berg and the sea ice. When they are moving in opposing directions (the angle θ between their velocity vectors satisfies $90° < \theta < 270°$), icebergs act as an obstacle, potentially slowing sea ice motion. The sea ice momentum equation

$$m\frac{d\mathbf{u}_i}{dt} = \mathbf{f}_R + \mathbf{f}_a + \mathbf{f}_w + \mathbf{f}_c + \mathbf{f}_{ss} + \mathbf{f}_{is} \tag{5}$$

is modified from its usual form by a berg-forcing term similar to $\mathbf{F}_{si}$ in equation (4)

$$\mathbf{f}_{is} = \frac{1}{2}\rho_b c_i A|\mathbf{u}_b - \mathbf{u}_i|(\mathbf{u}_b - \mathbf{u}_i), \tag{6}$$

where A represents the area of the sea ice/iceberg contact interface. For simplicity, we compute this quantity by multiplying the cross section perpendicular to the flow (i.e., the diameter of the berg) by the sea ice thickness. $\mathbf{f}_{is}$ is applied upstream (with respect to sea ice motion) of each iceberg, as illustrated in Figure 1a. In equation (5), $\mathbf{f}_R$ represents the sea ice rheology [*Hunke and Dukowicz*, 2002]; the remaining terms are equivalent to those in equation (1). Although the presence of an iceberg locked into compact sea ice likely would affect the drag on the ice pack with the addition of a form drag as in equations (2) and (3), we have not altered $\mathbf{f}_a$ or $\mathbf{f}_w$ in equation (5) from the standard CICE formulation.

[21] When a berg and the local sea ice are moving in a similar direction ($-90° < \theta < 90°$), $\mathbf{f}_{is}$ causes a numerical feedback in which the sea ice and iceberg accelerate one another, leading to model instability. Therefore, in this case we set $\mathbf{f}_{is} = 0$, and the berg ridges the area of sea ice that would otherwise be displaced due to the berg's motion relative to the sea ice

$$\Delta A = 2R\Delta t_b|\mathbf{u}_b - \mathbf{u}_i|, \tag{7}$$

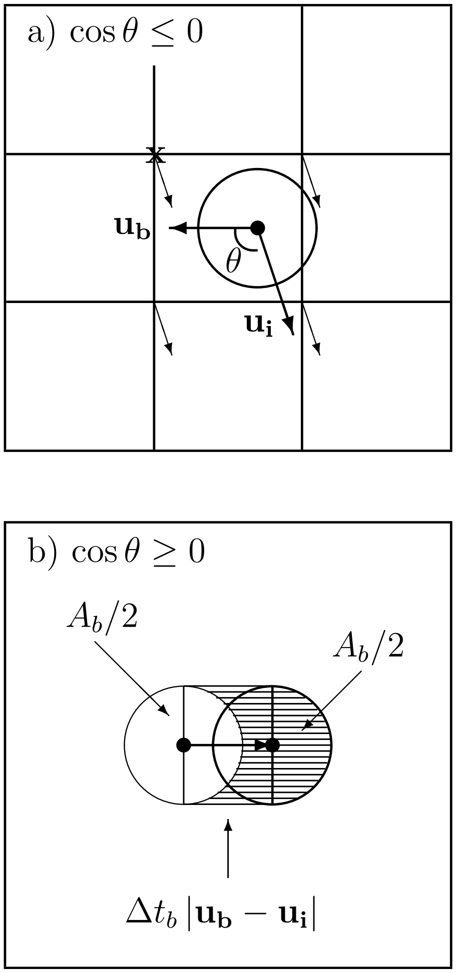

Figure 1. (a) An iceberg with velocity $\mathbf{u}_b$ moving in a direction opposing the sea ice velocity, given at the corners of the grid cell and interpolated to the center of the iceberg ($\mathbf{u}_i$) for use in the iceberg momentum equation. Both $\mathbf{u}_b$ and $\mathbf{u}_i$ are exaggerated. If the angle θ between $\mathbf{u}_b$ and $\mathbf{u}_i$ satisfies $\cos\theta < 0$, then the term $\mathbf{f}_{is}$ is interpolated to and applied at grid nodes where the sea ice velocity points into the grid cell, here marked with **x**. (b) When $\cos\theta > 0$, movement of the iceberg relative to the sea ice induces ridging of sea ice within the hatched region. The area of this region, ΔA, is given by the total area enclosed by the boundaries of the initial berg location (open circle), the final berg location (bold circle), and the tangent lines between them, less the area of the (initial) berg, A_b: $\Delta A = (A_b/2 + 2R\Delta t_b\ |\mathbf{u}_b - \mathbf{u}_i| + A_b/2) - A_b = 2R\Delta t_b\ |\mathbf{u}_b - \mathbf{u}_i|$.

where R is the iceberg radius and Δt_b is the time step, as illustrated in Figure 1b. That is, if the relative motion of the berg and the sea ice causes compression of the sea ice, the sea ice will buckle and pile up into ridges [e.g., *Rothrock*, 1975]. Any open water within this area closes before sea ice ridging begins, as in the standard CICE ridging scheme [*Lipscomb et al.*, 2007].

[22] Additionally, when sea ice is transported, the areas of the grid cells containing icebergs are reduced by the iceberg area, so that the sea ice occupies only the remaining portion of the grid cell. This effectively forces the ice to ridge more when entering a cell containing an iceberg.

3. Results

3.1. Iceberg Trajectories

[23] Four icebergs were initialized on 5 March 1990 in the eastern Weddell Sea, near and north of the concurrent location of iceberg C-7, and 1° apart in latitude. The track of C-7 is shown in Figure 2, in blue, from data provided by the National Ice Center (T. Arbetter, personal communication, 2009). Just 26 latitude-longitude locations are provided over the 22 months of C-7 data plotted here, resulting in long, linear segments where the time interval between observations is large. The dimensions of C-7 remained at 20 nautical miles × 10 nautical miles, or 686 km^2, throughout this period.

[24] In the control simulation, using the full sea ice and iceberg momentum equations including all interaction terms, the southerly berg (in red), which begins closest to the C-7 track, becomes grounded near the coast (Figure 2). Because of the relatively low grid resolution of these simulations (1°), the Antarctic coastal current is not well resolved in the ocean forcing data and is wider than observed. This weakens the sea surface tilt, which in turn affects the iceberg trajectories; for giant icebergs, forcing terms that include ice mass, such as Coriolis and sea surface tilt, dominate the momentum balance.

[25] Furthermore, we find that small changes in the model may cause the icebergs to take strikingly different paths, mainly due to their interaction with the bathymetry. *Bigg et al.* [1997] and *Lichey and Hellmer* [2001] both note chaotic behavior of their simulations when changing the dates of iceberg release in their models (which essentially alters the forcing data). As a result, *Bigg et al.* [1997] concludes

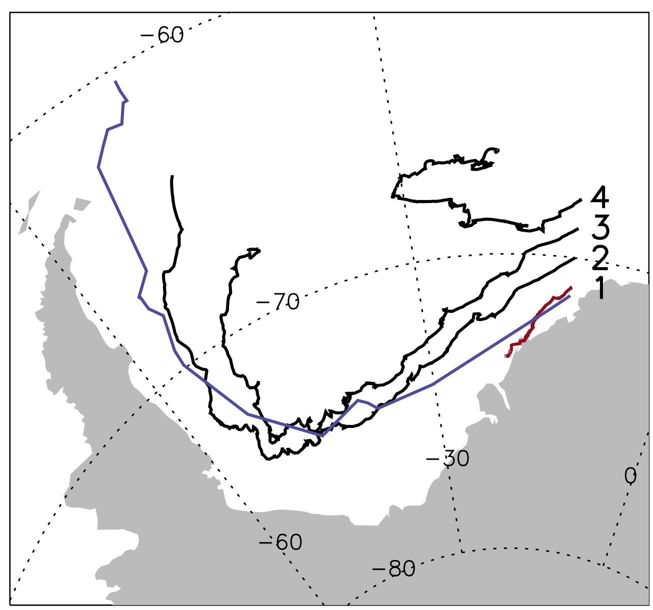

Figure 2. Iceberg tracks for 1990–1992 using the standard configuration. The blue line is the observed track of berg C-7. The icebergs are labeled 1–4 next to their starting positions.

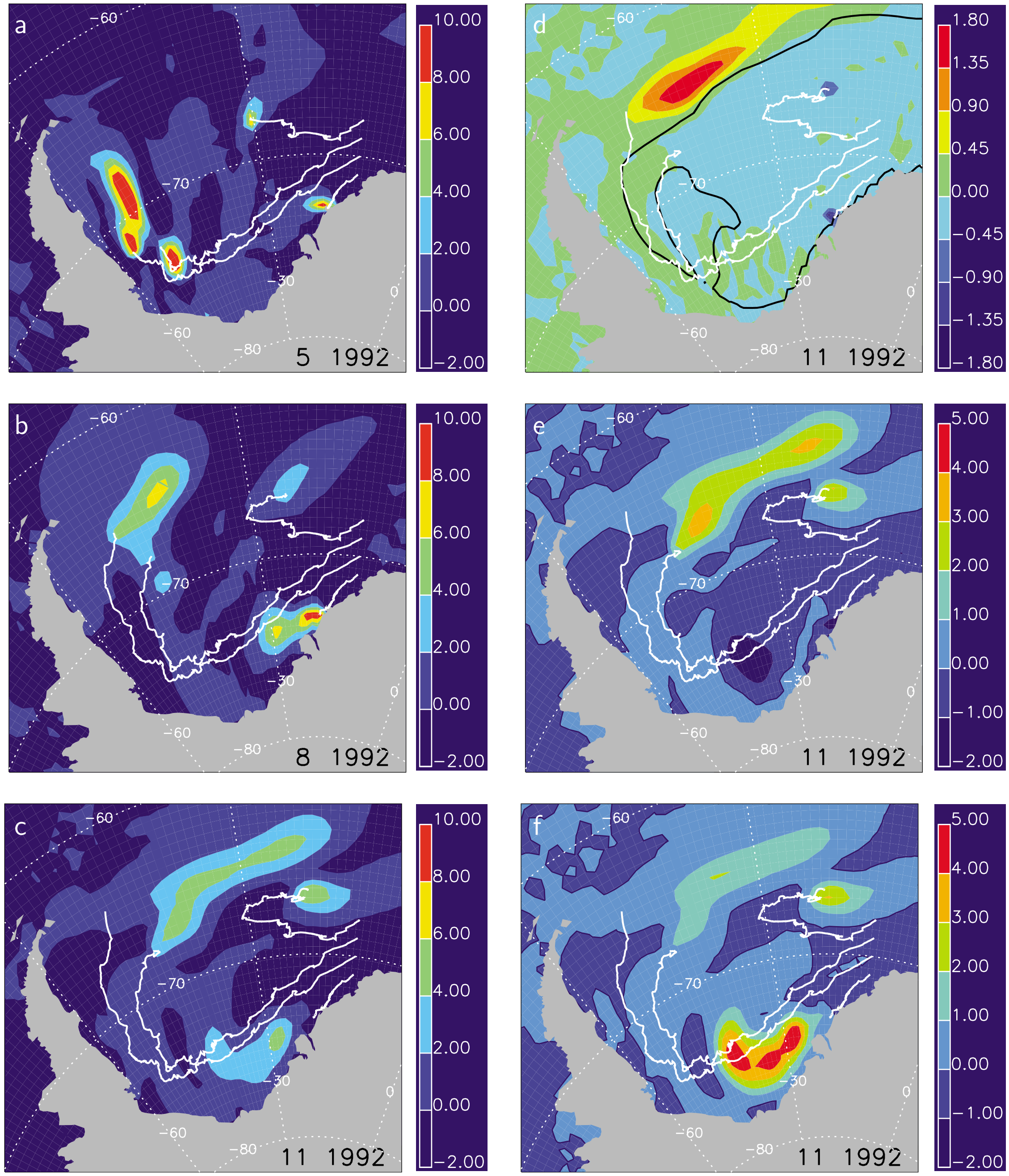

Figure 3. Differences between simulations with and without bergs. Thickness differences in cm for (a) May, (b) August, and (c) November 1992. Differences in (d) area (%), (e) ridged ice mean thickness (cm), and (f) level ice mean thickness (cm) for November 1992. White contours indicate the four berg tracks for the standard run, and the black curve in Figure 3d is the 90% ice area contour.

that "reproduction of any real, individual iceberg track would be extremely unlikely." Nevertheless, our bergs demonstrate the same behavior as C-7, moving slowly when there is little sea ice nearby and much faster in the winter, due to the "capturing" mechanism. Our iceberg tracks are in broad agreement with the observations of *Schodlok et al.* [2006] and quite similar to the simulations of *Lichey and Hellmer* [2001].

[26] Our goal in this paper is to answer the questions, (1) How might icebergs and sea ice be made to interact dynamically within a large-scale modeling context, and (2) what effect might this interaction have on the sea ice? Since our trajectories are qualitatively similar to those of *Lichey and Hellmer* [2001], and because precise iceberg trajectories are not essential to this study, we consider the simplifications to our iceberg model justified and the iceberg simulations appropriate for our use.

3.2. Sea Ice Distribution

[27] All of the bergs shed anomalies in the sea ice concentration and thickness which are transported with the sea ice flow (Figure 3). Sea ice speed is very similar in simulations with and without bergs (not shown), but resulting

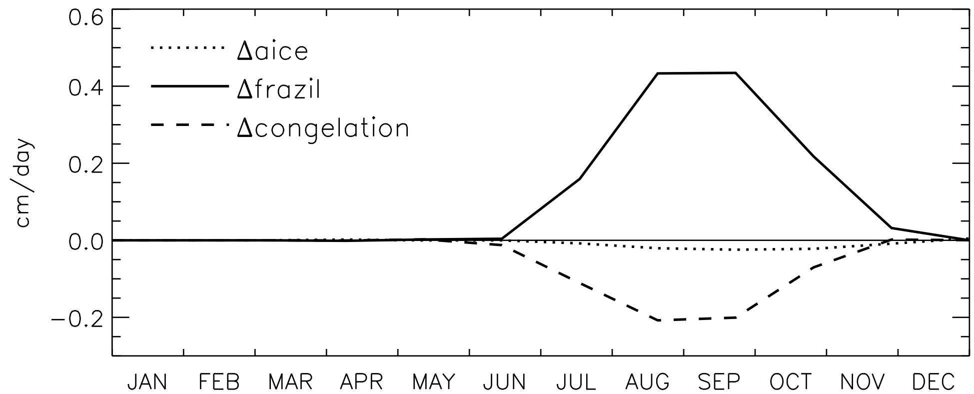

Figure 4. Difference in ice area fraction, frazil, and congelation ice growth downstream of iceberg 1 between the standard simulation with four bergs and the simulation without bergs for 1992. Ice growth units are cm d^{-1} as indicated on the y axis; area fraction is unitless.

differences in sea ice deformation, though highly localized, build up over time. These anomalies appear to precede the bergs, which are moving more slowly than the surrounding sea ice. Thus, sea ice differences generated at the berg location are transported ahead of the berg and stretched with the flow.

[28] Not surprisingly, the character of these differences depends on whether the iceberg is moving with the sea ice and on its position relative to the ice edge. For example, Figure 3d shows that berg 2 creates a large region of increased concentration near the ice edge, while the other bergs reduce the local ice area. Meanwhile, berg 3 induces more sea ice ridging (Figure 3e) and also thicker level ice (Figure 3f). However, berg 1, which is grounded near the coast during all of 1992, causes much more level ice to form than the others, little of which ridges. In fact, the greater open water areas evident in Figure 3d for bergs 1, 3, and 4 all result in more level ice growth.

[29] Figure 4 quantifies the increase in level ice production due to reduced area concentration just downstream of berg 1. While the difference in area fraction is very small, cold air temperatures lead to much larger heat fluxes over the open water area, which cool the ocean mixed layer and increase the amount of frazil ice produced by the ocean. With a smaller area of thicker sea ice present, the mean freezing rate of congelation ice, which forms on its underside due to upward heat conduction, declines.

[30] The differences shown in Figure 3 accumulate through the winter, reaching maximum spatial effect in the spring. The summer sea ice meltback largely decouples anomalies from one year to the next except in the perennial ice pack, which is too small in extent in this simulation [*Hunke*, 2010]. In the winter, sea ice area coverage is near 100% in all simulations, and therefore differences are seen only in the thickness fields. During fall and spring the sea ice area changes quickly as the ice edge advances and retreats, and thus some differences may be in the timing of when the ice edge crosses a given point.

[31] Table 2 provides sea ice volume anomalies and compares them with the total sea ice volume in the Southern Hemisphere, as simulated for November 1992. (Because the Southern Ocean sea ice pack is primarily seasonal, we compare the time-integrated net volume in the spring rather than volume production through the year.) The control run, shown in the first row of Table 2, produces anomalies that are a small fraction of 1% of the total volume. The anomaly would still be less than 1% if compared for just the Weddell Sea, which contains approximately one-third of the total Antarctic sea ice volume.

[32] Figure 5 highlights the model's response to the dynamic interaction processes. For instance, when the sea ice momentum term $\mathbf{f}_{is}$ is set to zero in equation (5), the resulting maximum ice thickness anomaly in November (Figure 5a) is larger than in the control run (Figure 3c). Here $\mathbf{f}_{is}$ is nonzero only when the iceberg and sea ice are moving toward each other; in that case sea ice motion is retarded, creating less open water for new ice formation. However with $\mathbf{f}_{is} = 0$, berg 1does not become grounded near the coast and produces a much smaller anomaly than in the standard configuration, leading to a smaller total anomaly in this case (Table 2, second row) than in the control run (Table 2, first row).

Table 2. Volume Anomalies for November 1992[a]

Icebergs	Total Berg Area (m^2)	Configuration	Sea Ice Volume Anomaly (km^3)	Total Sea Ice Volume (%)
4 giant	2.744×10^9	standard	24.7	0.23
4 giant	2.744×10^9	$\mathbf{f}_{is} = 0$	20.0	0.19
4 giant	2.744×10^9	no ridging	2.1	0.02
4 giant	2.744×10^9	all ridging	40.0	0.37
4 small	2.744×10^8	standard	4.1	0.04
1 giant	0.686×10^9	standard	9.1	0.09
40 small	2.744×10^9	standard	50.8	0.48

[a]Icebergs are located in the Weddell Sea, except for the 40-berg case, in which the bergs are spread around the entire Antarctic continent. The first row corresponds to Figure 3c; the second–fifth rows correspond to Figures 5a–5d, respectively.

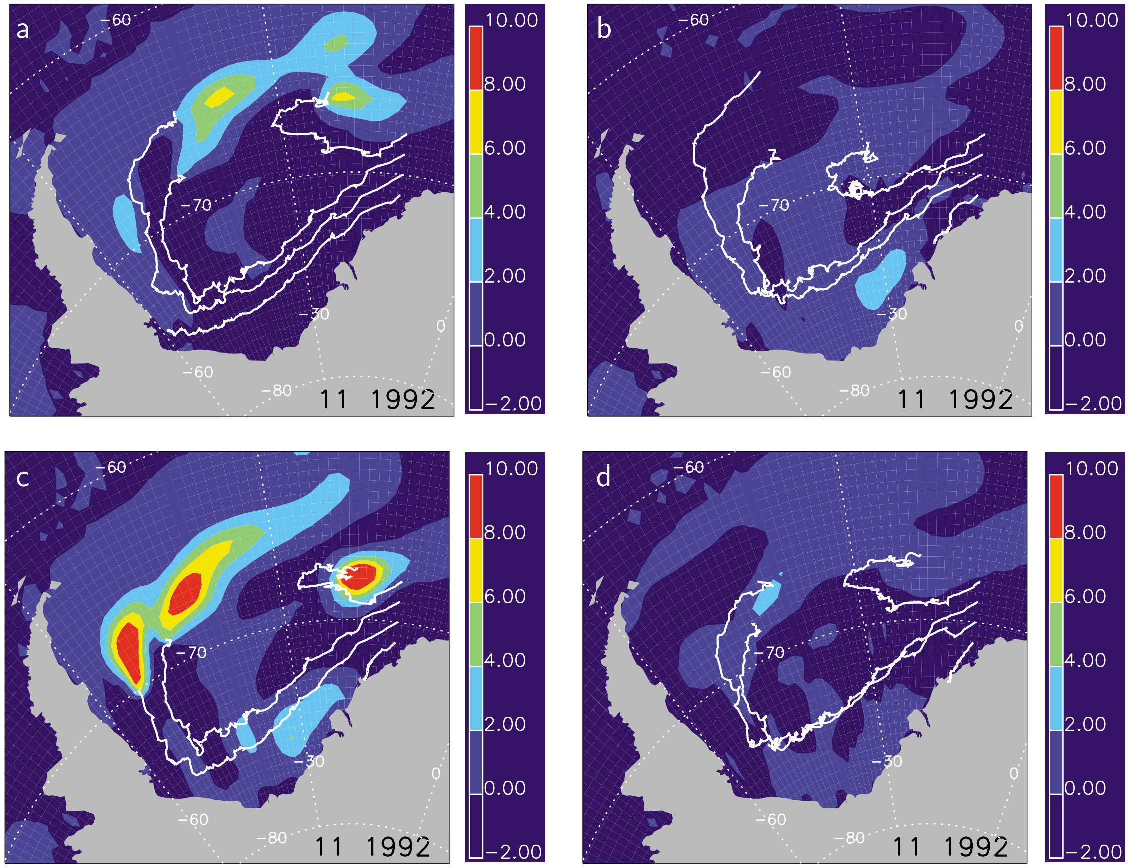

Figure 5. Sea ice thickness differences in cm between sensitivity simulations and the run without icebergs, for comparison with Figure 3c: (a) $\mathbf{f}_{is}$ = 0, (b) no sea ice ridging due to relative iceberg motion, (c) $\mathbf{f}_{is}$ replaced with full ridging interaction, and (d) smaller bergs.

[33] On the other hand, if $\mathbf{f}_{is}$ is retained but the sea ice is not allowed to ridge due to its motion relative to the berg when they are moving in similar directions (i.e., set $\Delta A = 0$ in equation (7)), the thickness changes very little compared with the no bergs run, except near the grounded berg (Figure 5b and Table 2, third row).

[34] If $\mathbf{f}_{is}$ is replaced with sea ice ridging (i.e., so that closing and/or ridging of the area given by equation (7) always occurs), the resulting thickness anomaly (Figure 5c and Table 2, fourth row) is larger than in the control run. In this case, the open water area created by the extra ridging reduces the ice strength enough that the three nongrounded bergs are caught by the sea ice pack less often, thus shortening their trajectories. In general, ridging caused by the relative motion of the sea ice and icebergs (as opposed to $\mathbf{f}_{is}$) tends to reduce the ice strength in the bergs' immediate surroundings.

[35] While only a few giant icebergs may be present in the Southern Ocean at any given time, there will be many more, smaller bergs. Figure 5d shows the change in ice thickness when the area of each iceberg is reduced by an order of magnitude to 68.6 km^2. The trajectories shown in Figures 3c and 5d are quite similar, considering that the iceberg mass is an order of magnitude different in the two simulations. This reflects the primary balance of the Coriolis and sea surface tilt terms, which include the iceberg mass and therefore dominate the momentum balance. Therefore we do not expect that our assumption of no thermodynamic melting significantly affects the trajectories [*Lichey and Hellmer*, 2001], at least in this configuration without an active ocean model component.

[36] Note that the volume anomaly produced by the four small icebergs (Table 2, fifth row) is not an order of magnitude smaller than in the control run. An additional sensitivity run using just one giant iceberg (berg 2 of the control run) demonstrates that the effects are not simply additive; the anomalies of the giant bergs influence each other. The smaller icebergs are less likely to interact, especially when spread around the entire continent (Table 2, seventh row). Forty small icebergs create a sea ice volume anomaly roughly an order of magnitude larger than that of four small bergs, and twice as large as the control case, in which four giant icebergs have the same mass (and cover the same ocean area fraction) as the 40 small ones. To better match the size distribution of *Silva et al.* [2006], additional 1 year simulations with 100 smaller bergs (the total berg area remaining identical) resulted in volume anomalies of the same order of magnitude as the run with 40 bergs (Table 2, seventh row).

[37] *Jacobs et al.* [1992] note that giant icebergs account for 50% of the total calving flux around Antarctica. For their iceberg trajectory model, *Gladstone et al.* [2001] estimated a calving flux of 1332 Gt yr^{-1}, excluding that of giant bergs. This flux is equivalent to 86 of our smaller icebergs, or

8.6 of our giant bergs. Taking this scaling factor into account and assuming (1) the “all ridging” case that produces the largest anomaly and (2) that the anomalies are not reduced through mutual interactions, we find that the total sea ice volume anomaly caused by 2664 Gt of icebergs would still be, at most, only a few percent of the total sea ice volume in the Southern Hemisphere at any given time. Moreover, our simulations indicate that sea ice volume anomalies are larger in the Weddell Sea than elsewhere because it contains a larger area of sea ice in which icebergs may move throughout the year.

4. Conclusions

[38] Our model development effort is spurred by two motivations. First, dynamical effects of icebergs on surrounding sea ice are observed. For instance, *Hunke and Ackley* [2001] note the presence of polynyas downstream of large, grounded bergs in both their observations and simulations of sea ice in the Weddell Sea. In the early 2000s, sea ice in the southern Ross Sea could not break out in the spring due to the presence of several large icebergs, causing stress on nearby penguin colonies [*Brunt et al.*, 2006; *Ainley et al.*, 2006]. Existing iceberg and sea ice models could not be utilized at that time to study this situation because they did not include the critical response of the sea ice to the presence of the icebergs. (Our current grid resolution is too coarse and our simplifications too broad for that particular case study.) Second, we are preparing for the time when ice sheets and glaciers will be fully incorporated in climate models, and icebergs must be accepted into the sea ice-ocean system as interactive thermodynamic and dynamic components.

[39] We have, for the first time, implemented dynamical forcing effects on sea ice by icebergs in a sea ice model widely used for large-scale climate simulations. We find that the effect of iceberg-sea ice dynamic interactions does make a difference locally and may be important for smaller-scale modeling studies, but the effect on climate-scale variables appears to be insignificant.

[40] The interaction implemented here represents the minimum possible, short of completely turning off the effect of bergs on sea ice. The differences shown here are strictly due to the dynamic interaction between ice bergs and sea ice; thermodynamic effects are not taken into account. Larger anomalies can be had by changing the manner in which the dynamic interaction occurs, for instance by making the sea ice ridge in the presence of icebergs directly, instead of modifying the sea ice motion via the momentum equation. However, while this approach may produce a factor of two in additional sea ice volume anomaly, the net effect will likely remain insignificant compared with the total sea ice volume production in the Southern Hemisphere.

[41] Inclusion of icebergs in the sea ice dynamics formulation will cause modifications to water, salt and heat exchanges with the ocean. Additional changes in sea ice volume associated with these ocean modifications are expected through thermodynamic feedback effects [e.g., *Jongma et al.*, 2009], and thus become a potential subject for future investigation. Based on our results, we expect that these additional changes will be small.

[42] The Lagrangian approach taken here for tracking icebergs is computationally expensive and not feasible for large numbers of bergs. In our simulations, each berg increased the total simulation runtime by about 10%. While standard optimization procedures were followed, the iceberg portion of the code was not highly optimized for these tests; a portion of the slowdown is due to poor load balancing in our particular berg configuration, with most of the iceberg calculations concentrated on one processor at any given time. Although meltwater distribution is important, we expect that precise iceberg trajectories will not be critical for future global climate simulations, and therefore a statistics based approach to simulating iceberg distributions is appropriate.

[43] **Acknowledgments.** This work was performed within the Climate, Ocean and Sea Ice Modeling (COSIM) project at Los Alamos National Laboratory, whose funding from the Biological and Environmental Research Division of the U.S. Department of Energy Office of Science is gratefully acknowledged. Marika Holland and David Bailey graciously provided the NCAR CCSM3 ocean forcing data set, and we thank Todd Arbetter of the National Ice Center for providing observed iceberg positions. Los Alamos National Laboratory is operated by the National Nuclear Security Administration of the U.S. Department of Energy under contract DE-AC52-06NA25396.

References

Ainley, D. G., G. Ballard, and K. M. Dugger (2006), Competition among penguins and cetaceans reveals trophic cascades in the western Ross Sea, *Ecology*, *87*, 2080–2093.

Bigg, G. R., M. R. Wadley, D. P. Stevens, and J. A. Johnson (1996), Prediction of iceberg trajectories for the North Atlantic and Arctic oceans, *Geophys. Res. Lett.*, *23*, 3587–3590.

Bigg, G. R., M. R. Wadley, D. P. Stevens, and J. A. Johnson (1997), Modelling the dynamics and thermodynamics of icebergs, *Cold Reg. Sci. Tech.*, *26*, 113–135.

Brunt, K. M., O. Sergienko, and D. R. MacAyeal (2006), Observations of unusual fast-ice conditions in the southwest Ross Sea, Antarctica: Preliminary analysis of iceberg and storminess effects, *Ann. Glaciol.*, *44*, 183–187.

Collins, W. D., et al. (2006), The Community Climate System Model Version 3 (CCSM3), *J. Clim.*, *19*, 2122–2143.

Gladstone, R. M., G. R. Bigg, and K. W. Nicholls (2001), Iceberg trajectory modeling and meltwater injection in the Southern Ocean, *J. Geophys. Res.*, *106*, 19,903–19,915.

Griffies, S. M., et al. (2009), Coordinated Ocean-ice Reference Experiments (COREs), *Ocean Modell.*, *26*, 1–46.

Harlow, F. H. (1955), A machine calculation method for hydrodynamic problems, *Report LAMS-1956*, Los Alamos Natl. Lab., Los Alamos, N. M.

Hibler, W. D. (1979), A dynamic thermodynamic sea ice model, *J. Phys. Oceanogr.*, *9*, 817–846.

Hunke, E. C. (2010), Thickness sensitivities in the cice sea ice model, *Ocean Modell.*, *34*, 137–149, doi:10.1016/j.ocemod.2010.05.004.

Hunke, E. C., and S. F. Ackley (2001), A numerical investigation of the 1997–98 Ronne Polynya, *J. Geophys. Res.*, *106*, 22,373–22,382.

Hunke, E. C., and J. K. Dukowicz (2002), The Elastic-Viscous-Plastic sea ice dynamics model in general orthogonal curvilinear coordinates on a sphere—Effect of metric terms, *Mon. Weather Rev.*, *130*, 1848–1865.

Hunke, E. C., and M. M. Holland (2007), Global atmospheric forcing data for Arctic ice-ocean modeling, *J. Geophys. Res.*, *112*, C04S14, doi:10.1029/2006JC003640.

Hunke, E. C., and W. H. Lipscomb (2008), CICE: The Los Alamos sea ice model, documentation and software user’s manual, version 4.0, *Tech. Rep. LA-CC-06-012*, Los Alamos Natl. Lab., Los Alamos, N. M.

Jacka, T. H., and A. B. Giles (2007), Antarctic iceberg distribution and dissolution from ship-based observations, *J. Glaciol.*, *53*, 341–356.

Jacobs, S. S., H. H. Hellmer, C. S. M. Doake, A. Jenkins, and R. M. Frolich (1992), Melting of ice shelves and the mass balance of Antarctica, *J. Glaciol.*, *38*, 375–387.

Jakobsson, M., N. Cherkis, J. Woodward, B. Coakley, and R. Macnab (2000), A new grid of Arctic bathymetry: A significant resource for scientists and mapmakers, *Eos Trans. AGU*, *81*, 89,93,96.

Jongma, J. I., E. Driesschaert, T. Fichefet, H. Goosse, and H. Renssen (2009), The effect of dynamic-thermodynamic icebergs on the Southern

Ocean climate in a three-dimensional model, *Ocean Modell.*, *26*, 104–113.
Keghouche, I., L. Bertino, and K. A. Lisaeter (2009), Parameterization of an iceberg drift model in the Barents Sea, *J. Atmos. Oceanic Technol.*, *26*, 2216–2227.
Kubat, I., M. Sayed, S. B. Savage, and T. Carrieres (2005), An operational model of iceberg drift, *Int. J. Offshore Polar Eng.*, *15*, 125–131.
Lichey, C., and H. H. Hellmer (2001), Modeling giant-iceberg drift under the influence of sea ice in the Weddell Sea, Antarctica, *J. Glaciol.*, *47*, 452–460.
Lipscomb, W. H., E. C. Hunke, W. Maslowski, and J. Jakacki (2007), Improving ridging schemes for high-resolution sea ice models, *J. Geophys. Res.*, *112*, C03S91, doi:10.1029/2005JC003355.
Lythe, M. B., and D. G. Vaughan (2001), BEDMAP: A new ice thickness and subglacial topographic model of Antarctica, *J. Geophys. Res.*, *106*, 11,335–11,351.
MacAyeal, D. R., M. H. Okal, J. E. Thom, K. M. Brunt, Y.-J. Kim, and A. D. Bliss (2008), Tabular iceberg collisions within the coastal regime, *J. Glaciol.*, *54*, 371–386.
Rothrock, D. A. (1975), The energetics of the plastic deformation of pack ice by ridging, *J. Geophys. Res.*, *80*, 4514–4519.
Savage, S. B. (2001), Aspects of iceberg deterioration and drift, in *Geomorphological Fluid Mechanics*, *Lect. Notes Phys. Ser.*, vol. 582, edited by N. J. Balmforth and A. Provenzale, pp. 279–318, Springer, Berlin.
Schodlok, M. P., H. H. Hellmer, G. Rohardt, and E. Fahrbach (2006), Weddell Sea iceberg drift: Five years of observations, *J. Geophys. Res.*, *111*, C06018, doi:10.1029/2004JC002661.
Silva, T. A. M., G. R. Bigg, and K. W. Nicholls (2006), Contribution of giant icebergs to the Southern Ocean freshwater flux, *J. Geophys. Res.*, *111*, C03004, doi:10.1029/2004JC002843.
Smith, S. D. (1993), Hindcasting iceberg drift using current profiles and winds, *Cold Reg. Sci. Tech.*, *22*, 33–45.
Smith, S. D., and E. G. Banke (1983), The influence of winds, currents and towing forces on the drift of icebergs, *Cold Reg. Sci. Tech.*, *6*, 241–255.
Smith, W. H., and D. T. Sandwell (1997), Global sea floor topography from satellite altimetry and ship depth soundings, *Science*, *277*, 1956–1962.

D. Comeau, Program in Applied Mathematics, University of Arizona, PO Box 210089, Tucson, AZ 85721-0089, USA.

E. C. Hunke, Fluid Dynamics and Solid Mechanics Group, Theoretical Division, Los Alamos National Laboratory, MS-B216, Los Alamos, NM 87545, USA. (eclare@lanl.gov)